AD-A071 450 GEORGE WASHINGTON UNIV WASHINGTON D C SCHOOL OF ENGI--ETC F/G 20/11
NONLINEAR DYNAMIC BUCKLING OF SPHERICAL CAPS WITH INITIAL IMPER--ETC(U)
JUN 79 R KAO N00014-75-C-0946

UNCLASSIFIED NL

1 OF 1
AD A071450

END
DATE FILMED
9-79
DDC

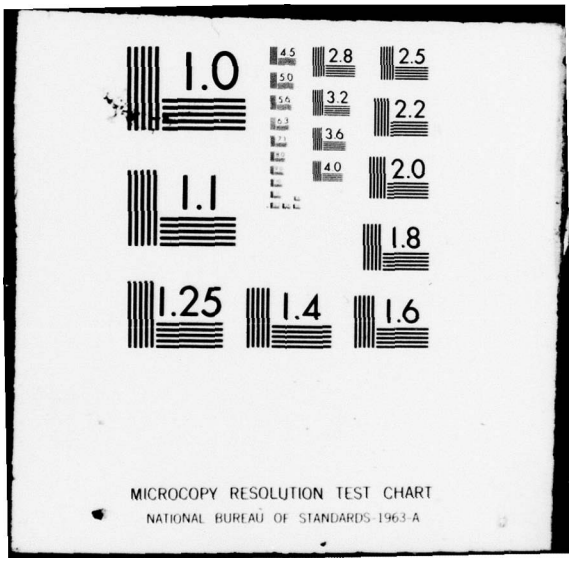
1.0
1.1
1.25
1.4
1.6
1.8
2.0
2.2
2.5
2.8
3.2
3.6
4.0
4.5
5.0
5.6
MICROCOPY RESOLUTION TEST CHART
NATIONAL BUREAU OF STANDARDS-1963-A

LEVEL II (6)

NONLINEAR DYNAMIC BUCKLING OF SPHERICAL CAPS WITH INITIAL IMPERFECTIONS

THE GEORGE WASHINGTON UNIVERSITY

AD A071450

DDC FILE COPY

STUDENTS FACULTY STUDY R
ESEARCH DEVELOPMENT FUT
URE CAREER CREATIVITY CO
MMUNITY LEADERSHIP TECH
NOLOGY FRONTIE ESIGN
ENGINEERING APP ENC
GEORGE WASHIN NIV

DDC
PROCESSED
JUL 20 1979
A

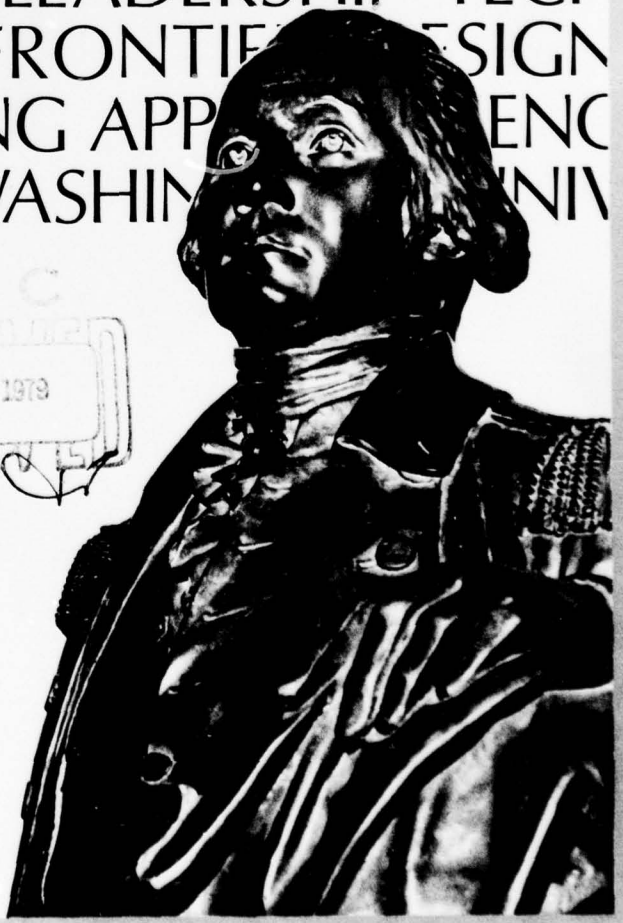

79 07 19 022

SCHOOL OF ENGINEERING
AND APPLIED SCIENCE

THIS DOCUMENT HAS BEEN APPROVED FOR PUBLIC RELEASE AND SALE: ITS DISTRIBUTION IS UNLIMITED

NONLINEAR DYNAMIC BUCKLING OF SPHERICAL CAPS WITH INITIAL IMPERFECTIONS

Robert Kao

Sponsored by
Office of Naval Research
Arlington, Virginia 22217

Contract Number
NAVY 00014-75-C-0946

June 1979

School of Engineering and Applied Science
The George Washington University
Washington, D.C. 20052

79 07 19 022

NONLINEAR DYNAMIC BUCKLING OF SPHERICAL CAPS WITH INITIAL IMPERFECTIONS[1]

By

Robert Kao

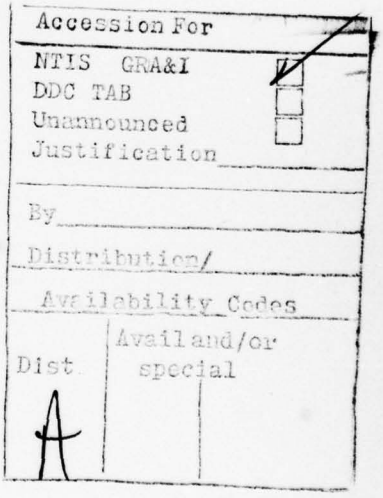

[1] The research reported on here was supported by the Office of Naval Research, Contract Number NAVY 00014-75-C-0946

ABSTRACT

A finite difference method is developed for the large deformation elastic-plastic dynamic buckling analysis of axisymmetric spherical caps with initial imperfections. The problem formulation is based on governing differential equations of motion, treating the plastic deformation as an effective plastic load. Both perfectly plastic and strain hardening behavior are implemented in the program. Strain hardening is incorporated through use of the Prager-Ziegler kinematic hardening rule, so that the Bauschinger effect is accounted for. The solution for the large deformation elastic-plastic dynamic response of a spherical cap is compared very favorably with other findings. Two spherical cap models are selected to study the title problem. Results obtained indicate that both plastic yielding and initial imperfection play significant roles in reducing the load carrying capacity of these shell structures. Both increase their influence as the thickness to radius ratio and the imperfection magnitude increase, respectively. It is also found that dynamic effect has the influence of lowering load carrying capacity of perfect spherical caps; however, its influence on imperfect spherical caps depends on the magnitude of initial imperfections.

INTRODUCTION

Dynamic buckling analysis of shell structures has been the subject of intense study. Shell structures designed according to quasi-static analysis may fail under conditions of dynamic loading. For a more realistic prediction on the load carrying capacity of these shells, in addition to the dynamic effect, considerations should also include other factors such as non-linearities in both material and geometry, initial imperfections, etc., since these factors, in a different manner, may also affect the magnitude of this capacity.

Large deformation dynamic buckling analysis was studied by several authors, notably Budiansky and Roth [1], Huang [2], Stephens and Fulton [3], Stricklin, et al. [4] and Ball and Burt [5]. A striking difference between the static and dynamic buckling analyses is on the buckling criterion. The dynamic snap-through, suggested in [1] and adopted in all these studies, is generally accepted as a means to obtain dynamic buckling loads of spherical caps under uniform step loading. Results of spherical caps obtained from these studies are in reasonable agreement.

Effect of initial imperfections on dynamic buckling loads of axisymmetric spherical caps was examined in Ref. [6]. It is found that initial imperfections do indeed have the effect of reducing the cap buckling capacity, and that the rate of change of the buckling load with respect to the imperfection is

greater when caps respond statically than dynamically. Two types of loading were also treated in Ref. [6], namely, step pressure of infinite duration and triangular pulses of various time durations. It is also revealed that the pulse duration has a very profound impact on the magnitude of the dynamic buckling load, and that the step loading of infinite duration, as a limiting case of triangular pulses, provides the most severe loading situation for the dynamic buckling analysis.

The combined effect of material and geometric nonlinearities on the shell behavior was studied by Marcal [7], Bushnell [8], Levine, et al. [9], and Kao [10]; the effect of initial imperfections was also considered in Ref. [10]. It is observed in Ref. [10] that both initial imperfection and plastic deformation have a similar influence of reducing shell load carrying capacity, and that the influence of plastic deformation decreases with increase of the imperfection magnitude. It is also found from this reference that the cap geometric parameter λ , an important factor in the elastic response, becomes meaningless in the elastic-plastic buckling analysis of spherical caps.

The purpose of this paper is to obtain large deformation elastic-plastic dynamic buckling loads of axisymmetric spherical caps with initial imperfections. The problem formulation is based on equilibrium equations of motion, treating the plastic deformation as an effective plastic load [10,11]. Governing equations are replaced by finite differences and a direct

method is applied for the time integration. At each time step, a relaxation technique [12] is introduced to solve nonlinear algebraic equations. Plasticity relations are derived from the incremental flow theory [13] together with the von Mises initial yield criterion and the Prager-Ziegler kinematic hardening rule [14,15]; this rule predicts an ideal Bauschinger effect.

In the next two sections, governing equations of motion and plasticity relations are subsequently given. This is followed by the description of the general solution procedure and dynamic buckling criteria. In the NUMERICAL RESULTS AND DISCUSSION section, first, the present solution of the large deformation elastic-plastic dynamic response of a spherical cap is compared with other findings; then, results of the title problem are presented and a general discussion on these results is given. Conclusions are outlined in the final section.

GOVERNING EQUATIONS OF MOTION

The geometry of a spherical cap is shown in Fig. 1a, in which H is the central height, R the shell radius and a is the base radius; W(r,t) and U(r,t) are the displacements along normal and tangential directions, respectively, and $W_i(r,0)$ is the initial imperfection; q(r,t) is the applied pressure. The undeformed shape of the perfect spherical cap can be adequately described by

$$Z = H\,[1 - (r/a)^2] \tag{1a}$$

where r is the radial coordinate. The radius of curvature of the shell is approximated by

$$R = a^2/2H \tag{1b}$$

Figure 1b shows an element with the stress resultants N_r and N_θ, the transverse shear Q_r and the moments M_r and M_θ. The equations of equilibrium including inertia forces in this element are

$$(rN_r)' - N_\theta = 0 \tag{2}$$

$$[rN_r (W_f - Z)' + rQ_r]' + rq = r\rho h\ddot{W} \tag{3}$$

$$(rM_r)' - M_\theta - rQ_r = 0 \tag{4}$$

where h is the shell thickness, ρ is the mass per unit volume of the shell and $W_f = W + W_i$; prime and dot denote differentiations with respect to r and t, respectively, and θ is the circumferential coordinate.

It is noted that, in light of the assumed shallowness, the effect of transverse shear Q_r and radial inertial force $r\rho h\ddot{U}$ in Eq. (2) is neglected, and that the nonlinearity has been introduced in Eq. (3) by considering the influence of W_f.

Eliminating Q_r in Eqs. (3) and (4), we obtain

$$M_r'' + \frac{2}{r} M_r' - \frac{1}{r} M_\theta' + N_r(W_f'' + \frac{1}{R}) + N_\theta(\frac{W_f'}{r} + \frac{1}{R}) + q = \rho h\ddot{W} \tag{5}$$

Eqs. (2) and (5) are the basic equations for the dynamic analysis of axisymmetric spherical caps in this paper. To

solve these two equations, we elect to express them in terms of the components U and W of the displacement. For this purpose, stress-strain and strain-displacement relations are required.

Stress-Strain and Strain-Displacment Relations

For a shell deforming into a plastic range, the strain in a point within the thickness can be considered as a combination of its elastic and plastic components:

$$\{e\} = \{e^e\} + \{e^p\} \tag{6}$$

where $\{e\}$, $\{e^e\}$ and $\{e^p\}$ are the total, elastic and plastic strain vectors, respectively. The total strain can also be expressed as a sum of the membrane and bending components:

$$\{e\} = \{\varepsilon\} + z\{\kappa\} \tag{7}$$

where z is the vertical coordinate through the shell thickness (Fig. 1b).

Membrane and bending strains are related to displacements by

$$\begin{aligned}
\varepsilon_r &= U' - \frac{W}{R} + \frac{1}{2}(W')^2 + W'W_i' \\
\varepsilon_\theta &= \frac{U}{r} - \frac{W}{R} \\
\kappa_r &= -W'' \\
\kappa_\theta &= -\frac{W'}{r}
\end{aligned} \tag{8}$$

Note that the elastic components of strains are the only strains which can be related to stresses by Hook's law:

$$\{\sigma\} = [E]\ (\{e\} - \{e^p\}) \tag{9}$$

where [E], the elastic strain to stress transformation matrix, is given as

$$[E] = \frac{E}{1-\nu^2}\begin{bmatrix} 1 & \nu \\ \nu & 1 \end{bmatrix} \tag{10}$$

in which E is Young's modulus and ν is Poisson's ratio.

Membrane stress resultants and bending moments are obtained by

$$\{N\} = \int_{-h/2}^{h/2} \{\sigma\} dz \tag{11}$$

$$\{M\} = \int_{-h/2}^{h/2} \{\sigma\} z dz \quad . \tag{12}$$

Substituting Eqs. (6-9) into Eqs. (11) and (12), we obtain the membrane forces

$$\begin{Bmatrix} N_r \\ N_\theta \end{Bmatrix} = \frac{Eh}{1-\nu^2} \begin{bmatrix} 1 & \nu \\ \nu & 1 \end{bmatrix} \begin{Bmatrix} \varepsilon_r \\ \varepsilon_\theta \end{Bmatrix} - \begin{Bmatrix} N_r^p \\ N_\theta^p \end{Bmatrix} \tag{13}$$

where the effective plastic membrane forces are

$$\begin{Bmatrix} N_r^p \\ N_\theta^p \end{Bmatrix} = [E] \int_{-h/2}^{h/2} \begin{Bmatrix} e_r^p \\ e_\theta^p \end{Bmatrix} dz \tag{14}$$

and the moments

$$\begin{Bmatrix} M_r \\ M_\theta \end{Bmatrix} = D\begin{bmatrix} 1 & \nu \\ \nu & 1 \end{bmatrix} \begin{Bmatrix} \kappa_r \\ \kappa_\theta \end{Bmatrix} - \begin{Bmatrix} M_r^p \\ M_\theta^p \end{Bmatrix} \tag{15}$$

where $D = Eh^3/12(1-\nu^2)$, and effective plastic moments are

$$\begin{Bmatrix} M_r^p \\ M_\theta^p \end{Bmatrix} = [E] \int_{-h/2}^{h/2} \begin{Bmatrix} e_r^p \\ e_\theta^p \end{Bmatrix} z\,dz \tag{16}$$

Governing Equations in Displacements

The governing equation involving the first major displacement U can now be obtained by substituting Eq. (13) into Eq. (2):

$$U'' + \frac{U'}{r} - \frac{U}{r^2} + G(W) = \frac{1-\nu^2}{Eh}\, q_1^p \tag{17}$$

where

$$\begin{aligned} G(W) &= F_r'(W) + \nu F_\theta'(W) + \frac{1-\nu}{r}(F_r - F_\theta) \\ F_r(W) &= -W/R + (W')^2/2 + W'W_i' \\ F_\theta(W) &= -W/R \\ F_r'(W) &= -W'/R + W'W'' + W'W_i'' + W''W_i' \\ F_\theta'(W) &= -W'/R \end{aligned} \tag{18}$$

and q_1^p, an effective plastic load, is related to effective plastic stress resultants by

$$q_1^p = (N_r^p)' + N_r^p/r - N_\theta^p/r \tag{19}$$

The second equation involving W as its major displacement can also be obtained by substituting Eq. (15) into Eq. (5):

$$D\nabla^4 W - \frac{Eh}{1-\nu^2}(\varepsilon_r+\nu\varepsilon_\theta)(W_f''+1/R) - \frac{Eh}{1-\nu^2}(\varepsilon_\theta+\nu\varepsilon_r)(W_f'/r + 1/R)$$

$$= q - q_2^p - q_3^p - \rho h\ddot{W} \tag{20}$$

where $\nabla^4 = \nabla^2(\nabla^2)$ and $\nabla^2\ (\ ) = (\ )'' + (\ )'/r$; the membrane strains $\varepsilon_r, \varepsilon_\theta$ are defined in Eqs. (8), effective plastic loads q_2^p and q_3^p are given as

$$q_2^p = N_r^p(W_f''+1/R) + N_\theta^p\ (W_f'/r+1/R) \tag{21}$$

$$q_3^p = (M_r^p)'' + 2(M_r^p)'/r - (M_\theta^p)'/r \tag{22}$$

Equations (17) and (20) are two fundamental governing equations in terms of displacements for the present analysis.

Boundary Conditions

At the shell apex, the nature of axisymmetry requires that

$$W'(0) = 0 \tag{23}$$

$$U(0) = 0 \tag{24}$$

Along the outer edge ($r = a$), if the cap is clamped:

$$U(a) = W(a) = W'(a) = 0\ . \tag{25}$$

On the other hand, if the cap is simply supported, it requires that

$$U(a) = W(a) = 0 \tag{26a}$$

and that $M_r(a)$ in Eq. (15) to be zero, i.e.

$$D\left(\frac{d^2W}{dr^2} + \frac{\nu}{r}\frac{dW}{dr}\right) = -M_r^p(a), \quad r = a \tag{26b}$$

where M_r^p is defined in Eq. (16).

Nondimensional Form

For convenience, following nondimensional quantities are introduced:

$$\begin{aligned}
x &= r/a & m^4 &= 12(1-\nu^2) \\
\lambda^2 &= m^2 a^2/Rh & q_{cr} &= 4Eh^2/R^2m^2 \\
(\,)' &= \partial(\,)/\partial x & p(r,t) &= q(r,t)/q_{cr} \\
(\dot{}) &= \partial(\,)/\partial\tau & u &= aU/h^2 \\
\tau &= \sqrt{E/\rho R^2}\; t & w &= W/h \\
w_i &= W_i/h
\end{aligned} \tag{27}$$

where q_{cr} is the classical buckling pressure of a complete spherical shell of the same radius of curvature and thickness.

By using Eq. (27), nondimensional forms of Eqs. (17) and (20) become

$$u'' + \frac{u'}{x} - \frac{u}{x^2} + g(w) = \frac{(1-\nu^2)a^3}{Eh^3}\, q_1^p \tag{28}$$

and

$$\nabla^4 w - 12(\bar{\varepsilon}_r+\nu\bar{\varepsilon}_\theta)\left(w''_f+\frac{\lambda^2}{m^2}\right) - 12(\bar{\varepsilon}_\theta+\nu\bar{\varepsilon}_r)\left(\frac{w'_f}{x}+\frac{\lambda^2}{m^2}\right)$$

$$= 4\frac{\lambda^4}{m^2}p - \frac{m^4\alpha^4}{Eh^4}(q_2^p+q_3^p) - \lambda^4\ddot{w} \qquad (29)$$

where g(w) and f(w) terms are nondimensional counterparts of similar terms in Eq. (18):

$$g(w) = f'_r(w) + \nu f'_\theta(w) + (1-\nu)[f_r(w) - f_\theta(w)]/x$$

$$f_r(w) = -\frac{\lambda^2}{m^2}w + \frac{1}{2}(w')^2 + w'w'_i$$

$$f_\theta(w) = -\frac{\lambda^2}{m^2}w \qquad (30)$$

$$f'_r(w) = -\frac{\lambda^2}{m^2}w' + w'w'' + w'w''_i + w''w'_i$$

$$f'_\theta(w) = -\frac{\lambda^2}{m^2}w'$$

and $\bar{\varepsilon}_r$, $\bar{\varepsilon}_\theta$ are nondimensional quantities of membrane strains ε_r and ε_θ in Eq. (8)

$$\bar{\varepsilon}_r = u' - \frac{\lambda^2}{m^2}w + \frac{1}{2}(w')^2 + w'w''_i$$

$$\qquad (31)$$

$$\bar{\varepsilon}_\theta = \frac{u}{x} - \frac{\lambda^2}{m^2}w$$

CONSTITUTIVE EQUATIONS OF PLASTICITY

The response of an elastic-plastic material can be described [15] by

(a) an initial yield condition, specifying the state of stress for which plastic flow first sets in,

(b) a flow rule, relating the plastic strain increment with the stress and the stress increment, and

(c) a hardening rule, specifying the subsequent yield condition in the course of plastic flow.

In this paper, the von Mises yield condition, which describes a smooth surface in stress space and represents a simple mathematical function, is chosen as the initial yield condition. The flow theory of von Mises and the Prager-Ziegler kinematic hardening rule are also selected; this rule predicts an ideal Bauschinger effect.

In a 9-space stress field with origin 0 (Fig. 2), the von Mises initial yield surface can be described by

$$F(\sigma_{ij}) = k^2 = \text{constant} \tag{32}$$

For an initially isotropic material, the form of the function F is invariant with respect to a rotation of the stress state.

The Prager's hardening rule [14] assumes that during plastic deformation, the yield surface moves in a translation without changing its shape and hence the subsequent yield surface takes the form

$$F(\sigma_{ij} - \alpha_{ij}) = k^2 \tag{33}$$

where α_{ij} represents the total translation of the yield surface center which is a measure of the degree of work hardening. In

the space σ_{ij}, α_{ij} is the position vector of the yield surface center C which before plastic deformation takes place is located at the origin (Fig. 2).

The flow rule of von Mises gives the following expression:

$$de^p_{ij} = \frac{\partial F}{\partial \sigma_{ij}} d\lambda \ , \ d\lambda > 0 \tag{34}$$

which indicates that the plastic strain increment de^p_{ij} lies in the exterior normal of the yield surface (33).

The Ziegler's modification [15] of Prager's hardening rule suggests that the surface (33) moves in the direction of the radius connecting its center with the stress point (Fig. 2):

$$d\alpha_{ij} = (\sigma_{ij} - \alpha_{ij}) d\mu \ , \ d\mu > 0 \tag{35}$$

$d\lambda$ in Eq. (34) and $d\mu$ in Eq. (35) are to be determined.

Determination of $d\mu$ is based on the condition that stress point always remains on the yield surface in plastic flow. This condition, in fact, states that for an infinitesimal increment of loading the vector $d\sigma_{ij} - d\alpha_{ij}$ must be orthogonal to the outer normal to the yield surface:

$$(d\sigma_{ij} - d\alpha_{ij}) \frac{\partial F(\sigma_{ij} - \alpha_{ij})}{\partial \sigma_{ij}} = 0 \ . \tag{36}$$

Substituting (35) into (36) yields

$$d\mu = \frac{(\partial F / \partial \sigma_{k\ell}) d\sigma_{k\ell}}{(\sigma_{mn} - \alpha_{mn}) \partial F / \partial \sigma_{mn}} \tag{37a}$$

and hence

$$d\alpha_{ij} = \frac{(\partial F/\partial\sigma_{k\ell})d\sigma_{k\ell}}{(\sigma_{mn}-\alpha_{mn})\partial F/\partial\sigma_{mn}}(\sigma_{ij}-\alpha_{ij}) \tag{37b}$$

According to Refs. [14,15], $\partial\lambda$ in (34) can be obtained by assuming $d\alpha_{ij} = cde^p_{ij}$ and putting this relation into (36):

$$d\lambda = \frac{1}{c}\frac{(\partial F/\partial\sigma_{k\ell})d\sigma_{k\ell}}{(\partial F/\partial\sigma_{mn})(\partial F/\partial\sigma_{mn})} \tag{38a}$$

and hence

$$de^p_{ij} = \frac{1}{c}\frac{(\partial F/\partial\sigma_{k\ell})d\sigma_{k\ell}}{(\partial F/\partial\sigma_{mn})(\partial F/\partial\sigma_{mn})}\frac{\partial F}{\partial\sigma_{ij}} \tag{38b}$$

where c is the hardening coefficient and can be determined from the uniaxial stress-strain relation.

Now, let us write Eq. (33) in terms of 3 principal stresses:

$$f = F - k^2$$

$$= \frac{1}{2}[(\bar{\sigma}_1-\bar{\sigma}_2)^2 + (\bar{\sigma}_2-\bar{\sigma}_3)^2 + (\bar{\sigma}_3-\bar{\sigma}_1)^2] - \sigma_y^2 = 0 \tag{39}$$

where σ_y is the yield stress in uniaxial tension and $\bar{\sigma}_1 = \sigma_1 - \alpha_1$, $\bar{\sigma}_2 = \sigma_2 - \alpha_2$, $\bar{\sigma}_3 = \sigma_3 - \alpha_3$.

For the case of plane stress (Fig. 3), we have

$$\sigma_3 = \alpha_3 = \bar{\sigma}_3 = 0 \tag{40}$$

and Eq. (39) reduces to

$$f = \bar{\sigma}_1^2 - \bar{\sigma}_1\,\bar{\sigma}_2 + \bar{\sigma}_2^2 - \quad^2 = 0 \quad . \tag{41}$$

By putting Eq. (39) into Eq. (38b) and using relations

(40-41), we obtain

$$\begin{Bmatrix} \Delta e_1^p \\ \Delta e_2^p \end{Bmatrix} = \frac{1}{D} \begin{bmatrix} S_1^2 & S_1 S_2 \\ S_1 S_2 & S_2^2 \end{bmatrix} \begin{Bmatrix} \Delta\sigma_1 \\ \Delta\sigma_2 \end{Bmatrix} \quad . \tag{42}$$

where

$$S_1 = (\bar{\sigma}_1 - \bar{\sigma}_2/2)\sigma_y \ , \ S_2 = (\bar{\sigma}_2 - \bar{\sigma}_1/2)/\sigma_y \ , \ D = \frac{3}{2} c \quad . \tag{43}$$

From Hook's law, we have

$$\begin{Bmatrix} \Delta\sigma_1 \\ \Delta\sigma_2 \end{Bmatrix} = \frac{E}{1 - \nu^2} \begin{bmatrix} 1 & \nu \\ \nu & 1 \end{bmatrix} \begin{Bmatrix} \Delta e_1^e \\ \Delta e_2^e \end{Bmatrix} \quad . \tag{44}$$

It is also noted that

$$\begin{Bmatrix} \Delta e_1^e \\ \Delta e_2^e \end{Bmatrix} = \begin{Bmatrix} \Delta e_1 \\ \Delta e_2 \end{Bmatrix} - \begin{Bmatrix} \Delta e_1^p \\ \Delta e_2^p \end{Bmatrix} \quad . \tag{45}$$

Introducing (42) into (44) provides

$$\begin{Bmatrix} \Delta\sigma_1 \\ \Delta\sigma_2 \end{Bmatrix} = \begin{bmatrix} C_{11} & C_{12} \\ C_{21} & C_{22} \end{bmatrix} \begin{Bmatrix} \Delta e_1 \\ \Delta e_2 \end{Bmatrix} \tag{46}$$

where

$$C_{11} = \frac{E}{\Omega} (D + E\, S_2^2)$$

$$C_{12} = \frac{E}{\Omega} (D\nu - E S_1 S_2) = C_{21}$$

$$C_{22} = \frac{E}{\Omega} (D + E\, S_1^2)$$

$$\Omega = D(1-\nu^2) + E(S_1^2 + 2\nu S_1 S_2 + S_2^2) \quad .$$

For a given displacement field, $\{\Delta e\}$ are obtained from incremental forms of Eqs. (7) and (8). Eqs. (46) are the stress-strain relations during the course of plastic flow (loading). Otherwise, Eqs. (44) should be used for all other stress computations.

Up to this point, the hardening coefficient c in Eq. (43) is the only constant yet to be decided. If the structure is in a state of uniaxial stress, the stress-strain relation is the same as that obtained from tension or compression tests. The expression for the hardening coefficient c can be readily obtained from Eq. (42) by setting $\Delta e^p = \Delta e_1^p$, $\Delta\sigma = \Delta\sigma_1$:

$$\frac{1}{c} = \frac{3}{2}\frac{\Delta e^p}{\Delta\sigma} \tag{47a}$$

or

$$D = \frac{\Delta\sigma}{\Delta e^p} \quad . \tag{47b}$$

This equation shows that the value of D is equal to the slope of the uniaxial stress-plastic strain curve.

From Eqs. (47), the values of the hardening coefficient for two special cases may be specified here: (i) for an elastic-ideally plastic material, $c = D = 0$, (ii) for a linear hardening material, $D = EE_t/(E-E_t)$, where E_t is the tangent modulus. Uniaxial stress-strain curves for these two types of hardening material are given in Fig. 4.

Nonlinear Hardening

Also given in Fig. 4 is the stress-strain curve for a nonlinear hardening material. Its D value, instead of being a constant, depends on the state of stress. One way of dealing with this rather complicate situation is based on the Ramberg-Osgood representation of a uniaxial stress-strain curve [18]:

$$e = \frac{\sigma}{E} + \frac{3\sigma}{7E}\left|\frac{\sigma}{\sigma_{0.7}}\right|^{n-1} \tag{48}$$

where $n = 1 + \frac{\log\,(17/7)}{\log\,(\sigma_{0.7}/\sigma_{0.85})}$,

e is the total strain, E is the slope of the linear portion of the stress-strain curve, and $\sigma_{0.7}$ and $\sigma_{0.85}$ are the stresses at which the curve has secant moduli of 0.7E and 0.85E, respectively.

It is understood that the nonlinear term in Eq. (48) is the plastic strain. D value of this material can be obtained as

$$D = \frac{7E}{3n}\left|\frac{\sigma_{0.7}}{\sigma}\right|^{n-1} . \tag{49a}$$

We may generalize this equation to a multiaxial state of stress [16,17]:

$$D = \frac{7E}{3n}\left|\frac{\sigma_{0.7}}{\bar{\sigma}}\right|^{n-1} \tag{49b}$$

where $\bar{\sigma}$, the effective stress, is defined as

$$\bar{\sigma} = \sqrt{\frac{3}{2}\,\sigma'_{ij}\,\sigma'_{ij}} \tag{50a}$$

in which σ'_{ij} is the deviatoric stress. For the case of plane stress,

$$\bar{\sigma} = \sigma_1^2 - \sigma_1\,\sigma_2 + \sigma_2^2 \quad . \tag{50b}$$

Loading Criteria

In the incremental solution procedure for elastic-plastic problems, in addition to the constitutive relations, it is necessary to have a loading/unloading criterion. For this purpose, let's define $\dot{f} = (\partial f/\partial\sigma_{ij})d\sigma_{ij}$, where f has been defined in Eq. (39). Loading, unloading and neutral loading are associated with the plastic state $f = 0$, and are characterized by $\dot{f} > 0$, $\dot{f} < 0$ and $\dot{f} = 0$, respectively. When loading or neutral loading takes place, Eq. (46) must be applied. On the other hand, Eq. (44) must be used when unloading occurs.

SOLUTION STRATEGY

For convenience, a simple flow chart is sketched in Fig. 5 to demonstrate the general solution procedure. The entire process, which is to obtain for a given applied load q (or p) an elastic-plastic transient response of axisymmetric spherical caps, is divided into two major loops, namely, the elastic solution and material property loops.

In the elastic solution loop, all material properties at a specific time τ are held constant. Consequently, the effective plastic loads, q_i^p in governing equations (28) and (29) are fixed and combined with the actual externally applied load q, the problem is thus reduced to an elastic large deformation problem.

The second time derivative of w in Eq. (29) is approximated by the Houbolt's third-order backwards difference expression [19]:

$$\ddot{w}(x,\tau) = (1/\delta^2)\,[2w(x,\tau) - 5w(x,\tau-\delta) + 4w(x,\tau-2\delta) - w(x,\tau-3\delta)] \qquad (51)$$

where $\delta = \Delta\tau$ is the equal time increment. The accuracy of this representation is of order δ^2. Special attention is devoted to the first few time steps where Eq. (51) cannot be applied directly. Before giving the expression for these first few time steps, we note that the initial conditions are of the form

$$w(x,0) = 0, \quad \dot{w}(x,0) = 0 \qquad (52)$$

From Eq. (52), expression of Eq. (51) for the first few time steps can readily be obtained [2] as

1) $\tau = 0$, $w(x,0) = 0$

2) $\tau = \delta$; since $\dot{w}(x,0) = 0$, we have $w(x,-\delta) = w(x,\delta)$ and hence $\ddot{w}(x,\delta) = (2/\delta^2)\,w(x,\delta)$

3) $\tau = 2\delta$; $\ddot{w}(w,2\delta) = (2/\delta^2)\,[w(x,2\delta) - 3w(x,\delta)]$

4) $\tau > 2\delta$, Eq. (9) can be applied directly.

At this point, central finite differences are used to transform Eqs. (28) and (29) to a discrete system of equations, and the nonlinear relaxation technique [12] is employed to solve these nonlinear equations. The iteration in this loop is considered converged when the average absolute change of u and w displacements at all points is less than .0001.

With the new displacement field $\{u\}^k$, the material properties must be updated so that the (nonlinear) stress-strain relation can be satisfied at all points over the shell surface and through the thickness. In the material property loop, the loading criterion is first checked. If the material point is in an unloading situation or still in the elastic range, Hook's law is used and the computation is very straight-forward.

If the material point is in a loading situation, incremental strains $\{\Delta e\}$ are computed from Eq. (7) by using $\{\Delta u\} = \{u\}^k - \{u\}^{k-1}$ (where k is the number of the material property loop, see Fig. 5), and $\{\Delta\sigma\}$ are computed from Eq. (46). Having obtained $\{\Delta\sigma\}$, we find new values of $\{\sigma\}$, $\{e^e\}$ and $\{e^p\}$. The effective plastic loads q_i^p are then evaluated from integration formulae (19), (21) and (22) through the use of a Simpson's rule (9 thickness points are used for the entire computation in this paper).

The material property is considered to be updated if average absolute change of displacements between the present and previous material property loop is less than 0.0005. Otherwise, the iteration goes to the elastic solution loop and the entire

operation is repeated until the material property and equilibrium equations are simultaneously satisfied.

In our numerical computation, the number of nodal points are selected such that a subsequent increase in nodal points does not significantly affect the magnitude of the static buckling load. With this consideration, 14 nodal points for $\lambda = 5$ and up to 22 points for $\lambda = 10$ are adopted.

A time step must also be selected very judiciously. A good selection is such that the results are within a desired accuracy, but not too small in light of computer time considerations. A reasonable compromise of equal time increments of $\delta = 0.10$ is used; this same time increment is also selected in Ref. [3].

The axisymmetric initial imperfection adopted in this study is of the dimple type which was also used in Ref. [6]. This type of imperfection is expressed mathematically as

$$w_i = (W_{i0}/h)(1 - x^2)^3 \tag{53}$$

where W_{i0} is the maximum imperfection which occurs at the shell apex. Selection of this expression is, in fact, quite arbitrary. However, it does provide an adequate description for actual shells since the important parameter is the maximum eccentricity and not the imperfection shape function.

DYNAMIC BUCKLING CRITERION

Criteria for dynamic axisymmetric buckling of the shallow spherical shell are not as well defined as for static buckling,

and require an evaluation of the transient response of the shell for various load levels.

The criterion adopted most widely (Refs. [1-6]) is based on plots of the peak nondimensional average displacement in time history, Δ_{max}, of the shell structure versus the amplitude of the load where Δ is the average displacement and has been defined [3,5,6] in dimensionless form as follows:

$$\Delta = \int_0^a rWdr \; / \; \int_0^a rZdr \tag{54}$$

The numerator is the volume generated by the shell deformation and the denominator is the constant volume under the cap.

For loads below the dynamic buckling load, where the nonlinearities are small, the relationship between Δ_{max} and the load amplitude is approximately linear. However, there may exist a certain value of load amplitude at which a very small increase in this amplitude produces a very large in Δ_{max}. This load is defined as the critical pressure for axisymmetric buckling.

NUMERICAL RESULTS AND DISCUSSION

In reference [10], a computer program was successfully developed for the large deformation elastic-plastic analysis of spherical caps with initial imperfections. This program is extended to include the dynamic effect for the calculation in

this paper. Before proceeding to obtain numerical results for the title problem, it is advisable to solve an example problem and compare the present result with other existing solutions. The comparison should be very meaningful if other solutions are obtained using complete different method and theory from the approach adopted herein.

Comparison with Other Solutions

The example problem considered here is the dynamic response of a shallow spherical shell subjected to a uniformly distributed external step pressure $q = 600$ lb/in.^{2} Geometric dimensions and material properties are outlined in Fig. 6. A total of 14 stations along radial direction, 9 thickness points and a time step of $\Delta t = 10^{-5}$ seconds are used for the calculation. The material is assumed to obey von Mises initial yield criterion with linear kinematic hardening.

The large deformation elastic-plastic dynamic response is presented in Fig. 6, which also shows the result obtained by assuming the cap to remain elastic throughout the analysis. The static, elastic-plastic solution is also given in this figure.

The effect of material nonlinearity on the dynamic behavior of the cap is significant. It is observed that the mean value about which the apex displacement oscillates is greater in the elastic-plastic situation compared to the elastic analysis wherein the vibration occurs around the static displacement.

Figure 6 also displays the solutions obtained by Nagarajan

and Popov [20] and Bathe, Ramm and Wilson [21]. Both solutions were based on the finite element formulation, von Mises yield condition with linear isotropic hardening and a Newmark generalized acceleration scheme. Despite differences in the solution method and theory employed, the comparison among these results is excellent. It is noted that the same time step (10^{-5}sec.) is also used in their computations.

With the validity of the computer program established for nonlinear dynamic analysis as demonstrated in this example, we now proceed to tackle the title problem in the following section.

Large Deformation Elastic-Plastic Dynamic Buckling of Spherical Caps

From Ref. [10], we find that the large deformation elastic-plastic response of axisymmetric spherical caps under static uniform loading is independent of cap geometric parameter λ, a factor used to characterize the elastic spherical cap behavior, and rather depends on individual geometric dimensions. In other words, two different spherical caps with the same λ value have the same load carrying capacity (p_{cr}) in elastic analysis, but may yield different magnitude of elastic-plastic buckling pressures.

According to this observation, two types of spherical caps studied in [10], with very much difference in geometrical dimensions, are selected again for the present analysis. They are identified as shells A and B in Figs. 7 and 8, respectively. All geometrical dimensions in shells A and B are fixed with

exception that the thickness can be varied. By selecting $h = 0.26$ in. and 0.0227 in. respectively for shells A and B, both caps yield the same geometrical parameter $\lambda = 5$, but have different values of the thickness to radius ratio ($h/R = 0.0104$ for shell A and 0.0048 for shell B). Material properties of both caps given in the figures are assumed to obey von Mises initial yield condition with linear kinematic hardening.

In Ref. [6], two types of dynamic loading were considered for the buckling analysis of elastic axisymmetric spherical caps: uniform step loading with infinite duration and a right triangular pulse with various time duration. Results obtained from this reference reveal that pulse duration has a very significant impact on the magnitude of the dynamic buckling load, and that the step loading provides a more severe loading situation than the right triangular pulse for dynamic analysis. Based on this conclusion, only uniform step loading with infinite duration is considered for the present analysis.

As mentioned in SOLUTION STRATEGY, a judicious choice of time step $\Delta\tau = 0.1$ is used for all computations in this paper. A total response time of $\tau = 50$ is also chosen so that if there is no sudden jump in the average displacement Δ or no convergence failure in iteration during this period of time, we assume that no buckling occurs at this load. Convergence criteria are specified in Fig. 5.

Some large deformation elastic-plastic dynamic response curves for shells A and B are shown in Figs. 7 and 8, respec-

tively, which also show shell A buckles at p_{cr} = 0.26 while shell B at 0.36. For comparison purposes, some data of interest are also listed here: both caps have the same elastic dynamic buckling load p_{cr} = 0.46 [6], while their elastic-plastic static buckling values are 0.31 for shell A and 0.50 for shell B [10].

According to these results, some observations may be in order. First, buckling loads for spherical caps of elastic material are related to their geometric parameter λ. Secondly, plastic yielding plays a significant role in reducing the buckling pressure of spherical caps; the influence of plastic yielding increases with increase of the thickness to radius ratio. For example, plastic yielding reduces the dynamic buckling pressure p_{cr} for shell B (h/R = 0.0048) from 0.46 to 0.36, a 22% reduction in buckling capacity. On the other hand, the reduction increases to 43% (from 0.46 to 0.26) for shell A (h/R = 0.0104). This indicates that the geometric parameter λ becomes meaningless in elastic-plastic analyses. Another important observation is that the dynamic effect also reduces the buckling pressure of spherical caps. This is evidenced by the fact that dynamic effect cuts down elastic-plastic buckling loads for shell A from p_{cr} = 0.31 to 0.26, for shell B from 0.50 to 0.36.

From dynamic response curves in Figs. 7 and 8, it is found that in the load range above the buckling pressure a larger load level requires a shorter response time to reach Δ_{max} or to generate convergence failure in iteration. This seems to be

true for all cases treated herein except for one situation which will be discussed when the case is encountered.

Because of having a greater thickness to radius ratio and hence being more sensitive to plastic deformation, shell A is selected to examine the effect of initial imperfections on the cap elastic-plastic dynamic buckling pressure. On the other hand, shell B is studied again to establish more evidence on how the effect of plastic yielding on the buckling pressure is influenced by the thickness to radius ratio.

By setting h = 0.0101 in. and 0.0057 in. for shell B of Fig. 8, two caps are obtained, one having $\lambda = 7.5$ and $h/R = 0.0021$ and the other $\lambda = 10$ and $h/R = 0.0012$. Large deformation elastic-plastic dynamic response curves displayed in Figs. 9 and 10 show that buckling loads are read as $p_{cr} = 0.43$ for $\lambda = 7.5$ and 0.46 for $\lambda = 10$, while their corresponding elastic dynamic values are 0.44 and 0.49, respectively [10]. Reduction in buckling loads because of plastic yielding in these two cases may be neglected. Insensitivity to plastic deformation in these situations may be attributed to the fact that as the thickness to radius ratio becomes smaller, the membrane effect tends to be more dominant. At the time when the cap buckles, the development of plastic deformation may be still very limited or of minor importance.

It is noted that Fig. 9 provides the first and only exception that a smaller load magnitude takes a shorter response time to reach Δ_{max} or to yield convergence failure in itera-

tion, although the difference between the maximum response times for p = 0.43 and 0.44 is negligible.

Now, let us examine the combined effect of nonlinearities in material and geometry and initial imperfections on the dynamic buckling of spherical caps. As already mentioned earlier, shell A of $\lambda = 5$, whose geometric and material properties are given in Fig. 7, is selected for this analysis. Three values of initial imperfections $W_{i0}/h = 0.1$, 0.5 and 1.0 imposing on the cap domain of shell A are considered. Dynamic response curves of these three cases are shown separately in Figs. 11, 12 and 13.

Buckling loads read from these figures are $p_{cr} = 0.25$, 0.17 and 0.13 for $W_{i0}/h = 0.1$, 0.5 and 1.0, respectively. These values together with those of static-elastic, dynamic-elastic and static elastic-plastic [6,10] are listed in Table 1 and plotted in Fig. 14. Also recorded in Table 1 for comparison purposes are some buckling loads obtained in Fig. 8 and Ref. [10] for shell B (λ=5).

Table 1. Buckling loads for two clamped spherical caps (shell A, $\lambda = 5$, Fig. 7; shell B, $\lambda = 5$, Fig. 8)

$\frac{W_{i0}}{h}$	Elastic shells A and B		Elastic-plastic shell A		shell B	
	Static [6]	Dynamic [6]	Static [10]	Dynamic	Static [10]	Dynamic
0	.64	.46	.31	.26	.50	.36
.1	.54	.39	.28	.25	.43	-
.5	.32	.28	.20	.17	.27	-
1.0	.15	.185	.12	.13	.15	-

Results exhibited in Fig. 14 show that imperfections do indeed have a significant impact in reducing buckling capacity for all cases considered here, although they are influenced in a different manner. The difference in buckling load reduction may be examined from two different bases. First, if the examination is focused on the same material property (elastic or elastic-plastic), the rate of change of the buckling pressure p_{cr} with respect to the imperfection W_{i0}/h is smaller for the dynamic response than for the static. As a result, the reduction of buckling loads due to dynamic effect decreases with increase of the imperfection magnitude.* As the imperfection exceeds a certain magnitude ($W_{i0}/h > 0.75$ and 0.85 for the elastic and elastic-plastic material, respectively), the dynamic buckling loads may be even higher than the corresponding static buckling values. This finding suggests that the statement -- the dynamic effect introduced by a time-dependent load can reduce the load carrying capacity of a structure [22] -- is true for the perfect spherical cap, but not necessarily true for the cap with initial imperfections.

Secondly, if the examination is centered on the same loading situation (static or dynamic), results in Fig. 14 clearly demonstrate that both plastic yielding and initial imperfection have the same effect of lowering the shell load carrying capacity. Figure 14 also shows that the imperfection

---

*This reduction is referring to the difference between static and dynamic buckling loads under the same material property and the same imperfection magnitude W_{i0}/h (see Fig. 14).

is a more dominant factor, since the influence of plastic yielding diminishes as the imperfection magnitude increases.

The informations discussed here are quite useful for spherical cap designs. A valid design of these structures should reflect the actual material property, consider both static and dynamic responses, and also take into account the estimated magnitude of imperfections in light of manufacturing considerations.

CONCLUSIONS

The objective of this paper is to obtain large deformation elastic-plastic dynamic buckling loads of axisymmetric spherical caps with initial imperfections. The problem formulation is based on governing differential equations of motion, treating the plastic deformation as effective plastic loads which are combined together with actual applied forces.

Equations of motion are converted into a discrete system of equations by replacing all spacewise derivatives with central finite differences and the second time derivative with a Houbolt's third-order backwards difference expression [19]. Resulting nonlinear algebraic equations are then solved by a step-by-step time integration scheme for displacements. At each step of integration, the solution procedure is divided into two major loops, namely, elastic solution and material property loops.

In the elastic solution loop, all material properties are

held constant and nonlinear equations are solved by the nonlinear relaxation technique [12]. In the material property loop, material properties are updated to correspond the new computed state of stress to the specified stress-strain relation. The procedure consisting these two loops is repeated until governing equations and the specified stress-strain relation are satisfied at all points over the shell surface and throughout the thickness. The solution procedure discussed here is sketched in Fig. 5 for references.

The plasticity relation adopted herein is an incremental flow theory which is based on von Mises initial yield condition and the Prager-Ziegler kinematic hardening rule. It is noted that this theory takes into account the Bauschinger effect and that the computer program developed for the present analysis is equipped to handle the material of elastic-perfectly plastic, linear and nonlinear hardening behavior. Nine thickness points and a Simpson rule are used for all numerical caiculations of plastic deformation in this paper. A dimple type of imperfections is selected which provides a quite adequite description of the local nature of spherical shells.

To verify the validity of the theory and the solution method employed, the procedure is applied to obtain the large deformation elastic-plastic dynamic response of a spherical cap (Fig. 6). The present solution along with those obtained by Nagarajan and Popov [20] and Bathe, Ramm and Wilson [21] are displayed in Fig. 6. Their solutions are based on a finite

element formulation, isotropic strain hardening and a Newmark time integration scheme. Despite differences in the theory and solution methods utilized, the comparison among these three sets of results is remarkably good.

The solution procedure is then applied to solve the title problem; two spherical cap models shown in Figs. 7 and 8 are chosen for the present analysis. The loading exerted on the cap surface is assumed to be a uniform step pressure of infinite duration. The results, which are given and discussed in great details in the previous section, may be summarized as follows:

(1) For axisymmetric spherical caps of elastic material, their static and dynamic buckling loads (p_{cr}) are function of cap geometric parameter λ. However, for caps of elastic-plastic material, these values are independent of λ. This means that two spherical caps, which have the same λ value but different geometric dimensions, may yield the same magnitude of buckling load (p_{cr}) if their materials are elastic; however, their p_{cr} values may be different if their materials are elastic-plastic. For example, Table 1 shows that if both shells A and B (both have $\lambda = 5$) are made of the elastic material, their static buckling loads are of the same magnitude ($p_{cr} = 0.46$); both also have the same dynamic buckling value ($p_{cr} = 0.46$). But when their materials are assumed to be elastic-plastic, the static buckling loads are 0.31 and 0.50, and the dynamic values are 0.26 and 0.36 for shells A and B, respectively.

(2) Plastic yielding plays a significant role in reducing

the buckling pressure of spherical caps. The influence of plastic yielding increases with increase of the thickness to radius ratio. This observation may be illustrated from Table 1 that plastic yielding reduces the dynamic buckling pressure p_{cr} for shell B (h/r = 0.0048) from 0.46 to 0.36, a 22% reduction in buckling capacity. On the other hand, this reduction increases to 43% (from 0.46 to 0.26) for shell A (h/R = 0.0104).

(3) For perfect spherical caps, dynamic effect has an influence of lowering their load carrying capacity. This can be seen from Table 1 that dynamic effect cuts down their elastic-plastic buckling loads (p_{cr}) from 0.31 to 0.26 and from 0.50 to 0.36 for shells A and B, respectively.

(4) For imperfect spherical caps, dynamic effect on their load carrying capacity depends on the magnitude of imperfections. For example, the elastic results of shell A (λ=5) displayed in Fig. 14 demonstrate that when imperfection W_{i0}/h is less than 0.75, its dynamic p_{cr} values are smaller than its static values. On the other hand, when W_{i0}/h exceeds 0.75, the situation is completely reversed. A similar situation is also observed for shell A of elastic-plastic material.

Finally, it may be concluded that a realistic design of spherical caps should be based on the actual material property, consider both static and dynamic responses, and take into account the estimated magnitude of imperfections in light of manufacturing considerations.

REFERENCES

[1] Budiansky, B. and Roth, R. S., "Axisymmetric dynamic buckling of clamped shallow spherical shells," TND-1510, 1962, NASA, pp. 597-606.

[2] Huang, N. C., "Axisymmetric dynamic snap-through of elastic clamped shallow spherical shells," AIAA Journal, Vol. 7, no. 2, Feb. 1969, pp. 215-220.

[3] Stephens, W. B. and Fulton, R. E., "Axisymmetric static and dynamic buckling of spherical caps due to centrally distributed pressure," AIAA Journal, Vol. 7, no. 11, Nov. 1969, pp. 2120-2126.

[4] Stricklin, J. A., et al., "Dynamic buckling of clamped spherical caps under step pressure loadings," AIAA Journal, Vol. 7, no. 6, June 1969, pp. 1212-1213.

[5] Ball, R. E. and Burt, J. A., "Dynamic buckling of shallow spherical shells," Journal of Applied Mechanics, June 1973, pp. 411-416.

[6] Kao, R. and Perrone, N., "Dynamic buckling of axisymmetric spherical caps with initial imperfections," Computers and Structures, Vol. 9, 1978, pp. 463-473.

[7] Marcal, P. V., "Large deflection analysis of elastic-plastic shells of revolution," AIAA Journal, Vol. 8, no. 9, September 1970.

[8] Bushnell, D., "Large deflection elastic-plastic creep analysis of axisymmetric shells," Numerical Solution of Nonlinear Structural Problems, Proceedings of ASME Winter Meeting, Nov. 1973.

[9] Levine, H. S., Armen, H., Jr., Winter, R. and Pifko, A., "Nonlinear behavior of shells of revolution under cyclic loading," Computers and Structures, Vol. 3, 1973, pp. 589-617.

[10] Kao, R., "Large deformation elastic-plastic buckling analysis of spherical caps with initial imperfections," Technical report, School of Engineering and Applied Science, The George Washington University, Washington, D.C., 1979.

[11] Lin, T. H., Theory of inelastic structures, John Wiley and Son, New York, 1968.

[12] Perrone, N. and Kao, R., "A general nonlinear relaxation technique for solving nonlinear problems in mechanics," Journal of Applied Mechanics, Vol. 38, no. 2, June 1971, pp. 371-376.

[13] Hill, R., The Mathematical Theory of Plasticity, Oxford University Press, 1950.

[14] Prager, W., "The theory of plasticity: A survey of recent achievements," (James Clayton Lecture), Proc. Instn. Mech. Engrs., Vol. 169, 1955, p. 41.

[15] Ziegler, H., "A modification of Prager's hardening rule," Quart. Applied Math., Vol. 17, no. 1, 1959.

[16] Armen, H., Jr., Pifko, A. and Levine, H. S., "Finite element analysis of structures in the plastic range," NASA CR-1649, Feb. 1971.

[17] Svalbonas, V. and Levine, H., "Numerical nonlinear inelastic analysis of stiffened shells of revolution," Vol. I - Theory Manual for STARS-2P Digital Computer Program, NASA CR-2559, July 1975.

[18] Ramberg, W. and Osgood, W. R., "Description of stress-strain curves by three parameters," NASA TN 902, 1943.

[19] Houbolt, J. C., "A recurrence matrix solution for the dynamic response of elastic aircraft," Journal of Aeronautical Science, Vol. 17, Sept. 1950, pp. 540-550.

[20] Nagarajan, S. and Popov, E. P., "Nonlinear dynamic analysis of axisymmetric shells," International Journal for Numerical Methods in Engineering, Vol. 9, 1975, pp. 535-550.

[21] Bathe, K., Ramm, E. and Wilson, E. L., "Finite element formulation for large deformation dynamic analysis," International Journal for Numerical Methods in Engineering, Vol. 9, 1975, pp. 353-386.

[22] Lock, M. H., Okubo, S., and Whittier, J. S., "Experiments on the snapping of a shallow dome under a step pressure load," AIAA Journal, Vol. 6, no. 7, July 1968, pp. 1320-1326.

SECURITY CLASSIFICATION OF THIS PAGE (When Data Entered)

REPORT DOCUMENTATION PAGE

READ INSTRUCTIONS BEFORE COMPLETING FORM

1. REPORT NUMBER	2. GOVT ACCESSION NO. / 3. RECIPIENT'S CATALOG NUMBER
4. TITLE (and Subtitle): NONLINEAR DYNAMIC BUCKLING OF SPHERICAL CAPS WITH INITIAL IMPERFECTIONS	5. TYPE OF REPORT & PERIOD COVERED / 6. PERFORMING ORG. REPORT NUMBER
7. AUTHOR(s): Robert Kao	8. CONTRACT OR GRANT NUMBER(s): NAVY 00014-75-C-0946
9. PERFORMING ORGANIZATION NAME AND ADDRESS: The George Washington University, School of Engineering & Applied Science, Washington, D.C. 20052	10. PROGRAM ELEMENT, PROJECT, TASK AREA & WORK UNIT NUMBERS
11. CONTROLLING OFFICE NAME AND ADDRESS: Office of Naval Research, Arlington, Virginia 22217	12. REPORT DATE: June 1979 / 13. NUMBER OF PAGES: 34
14. MONITORING AGENCY NAME & ADDRESS (if different from Controlling Office)	15. SECURITY CLASS. (of this report): UNCLASSIFIED / 15a. DECLASSIFICATION/DOWNGRADING SCHEDULE

16. DISTRIBUTION STATEMENT (of this Report)

APPROVED FOR PUBLIC RELEASE: DISTRIBUTION UNLIMITED

17. DISTRIBUTION STATEMENT (of the abstract entered in Block 20, if different from Report)

18. SUPPLEMENTARY NOTES

19. KEY WORDS (Continue on reverse side if necessary and identify by block number)

Dynamic buckling	Initial imperfections
Step loading	Spherical caps
Large deformation	von Mises initial yield condition
Plastic yielding	Bauschinger effect
Kinematic hardening	Finite differences

20. ABSTRACT (Continue on reverse side if necessary and identify by block number)

A finite difference method is developed for large deformation elastic-plastic dynamic buckling analysis of imperfect spherical caps. The problem formulation is based on governing equations of motion, treating plastic deformation as effective plastic loads. Plasticity theory is derived from von Mises yield condition and Prager-Ziegler kinematic hardening rule which predicts an ideal Bauschinger effect. Results indicate that dynamic effect has the influence of reducing load carrying capacity of perfect spherical caps; however, its influence on imperfect caps depends on the magnitude of initial imperfections.

DD FORM 1 JAN 73 1473 EDITION OF 1 NOV 65 IS OBSOLETE
S/N 0102-014-6601

SECURITY CLASSIFICATION OF THIS PAGE (When Data Entered)

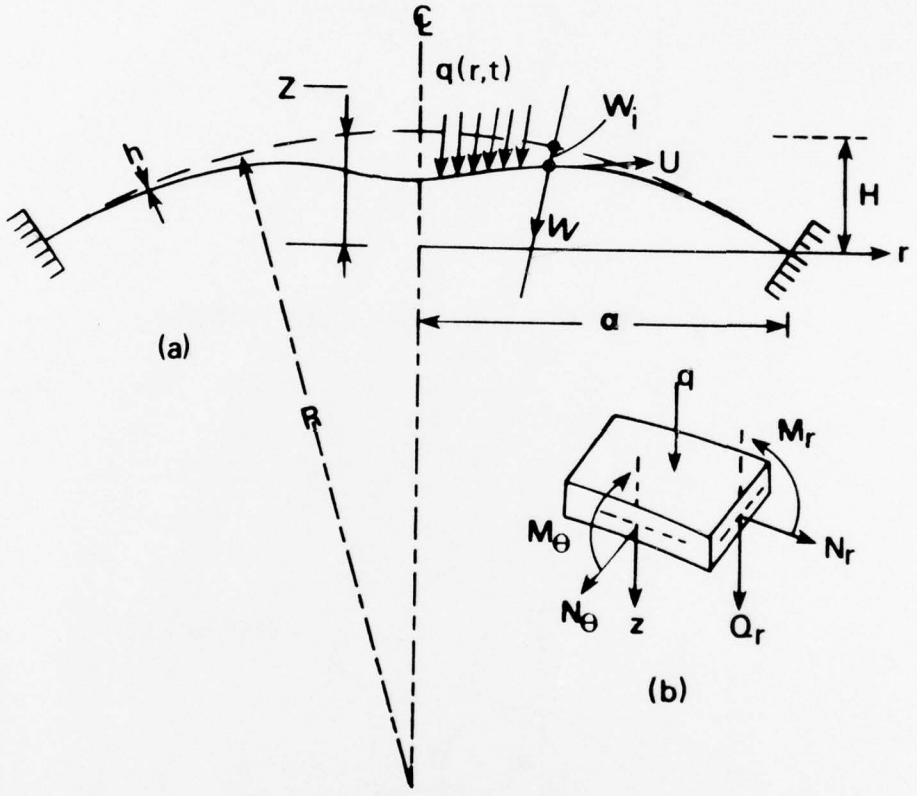

Fig. 1 – Geometry, stress resultants and moments for axisymmetric clamped spherical cap with initial imperfection.

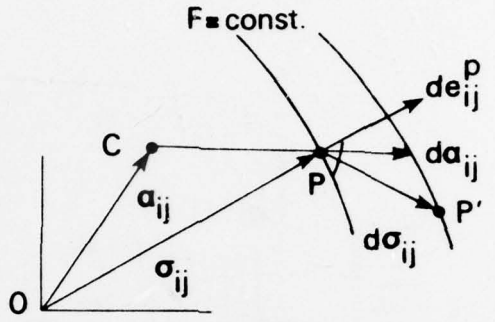

Fig. 2 – Flow rule and kinematic hardening.

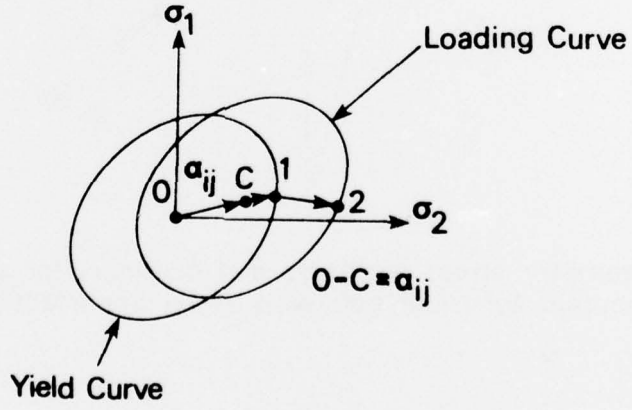

Fig. 3 – Kinematic hardening in plane stress.

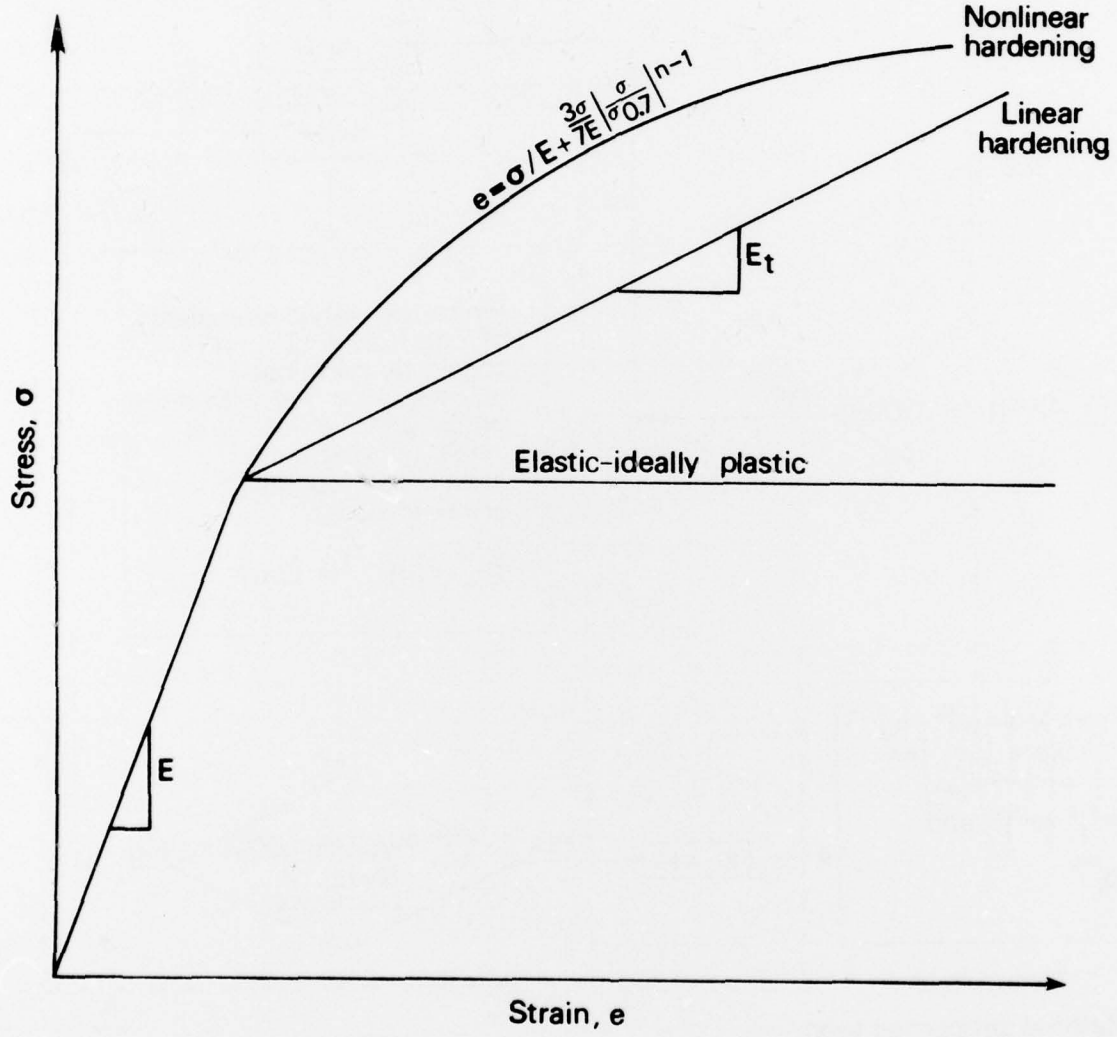

Fig. 4 – Nonlinear stress–strain curves (three types of hardening).

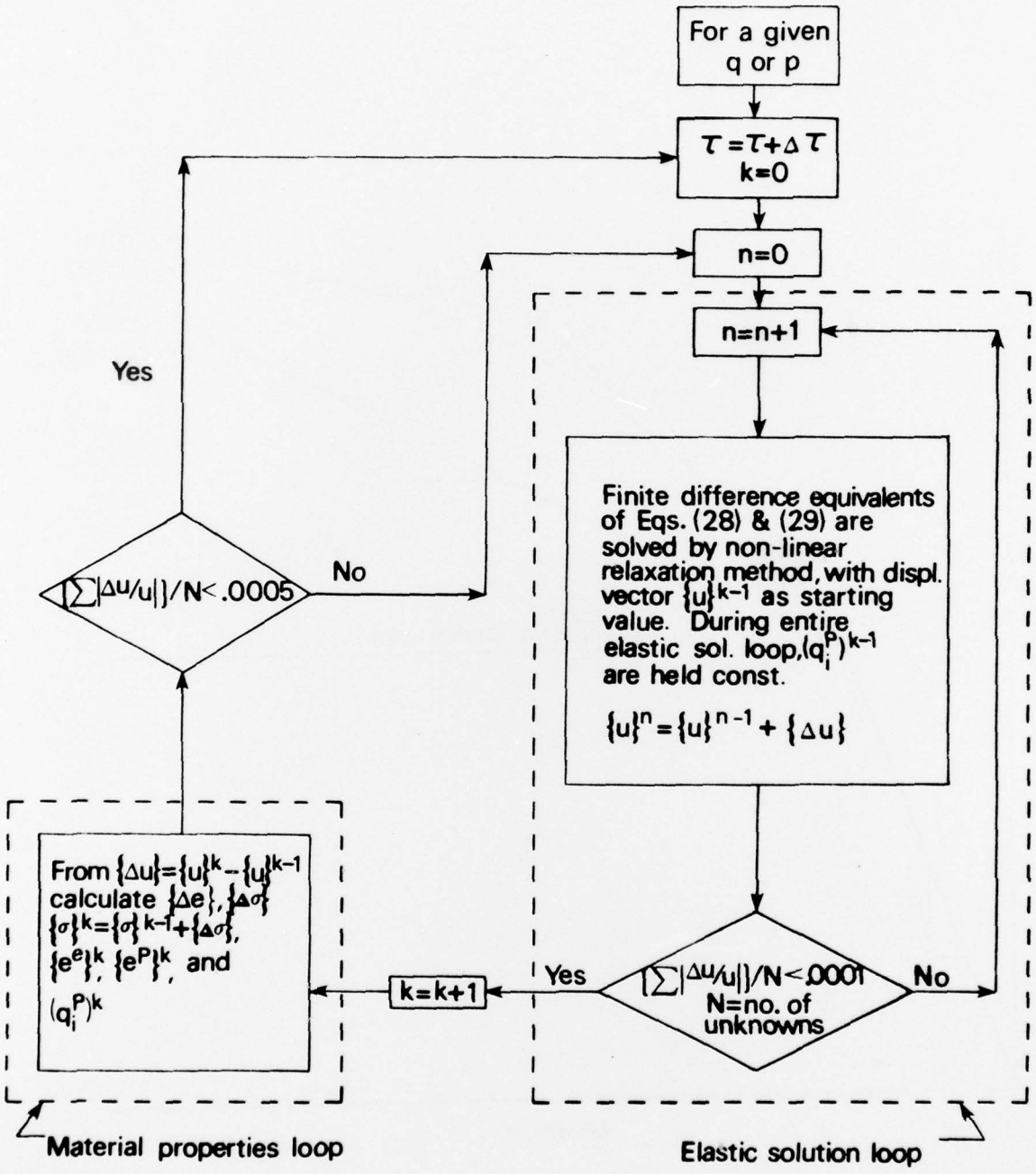

Fig. 5 – Iteration procedure for large deformation elastic-plastic dynamic problems.

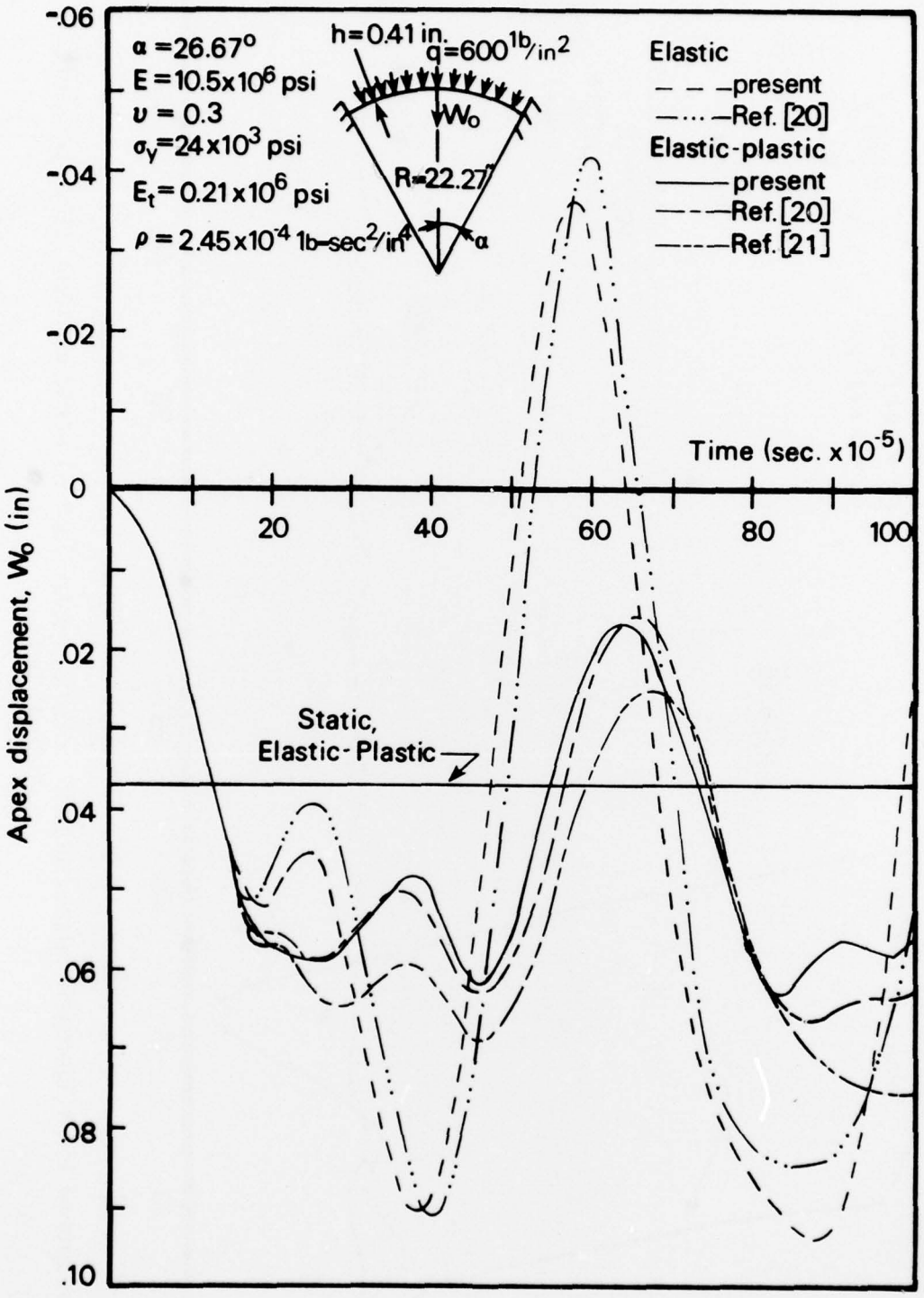

Fig. 6. Large displacement dynamic elastic-plastic analysis of spherical cap under uniform external pressure of 600 psi.

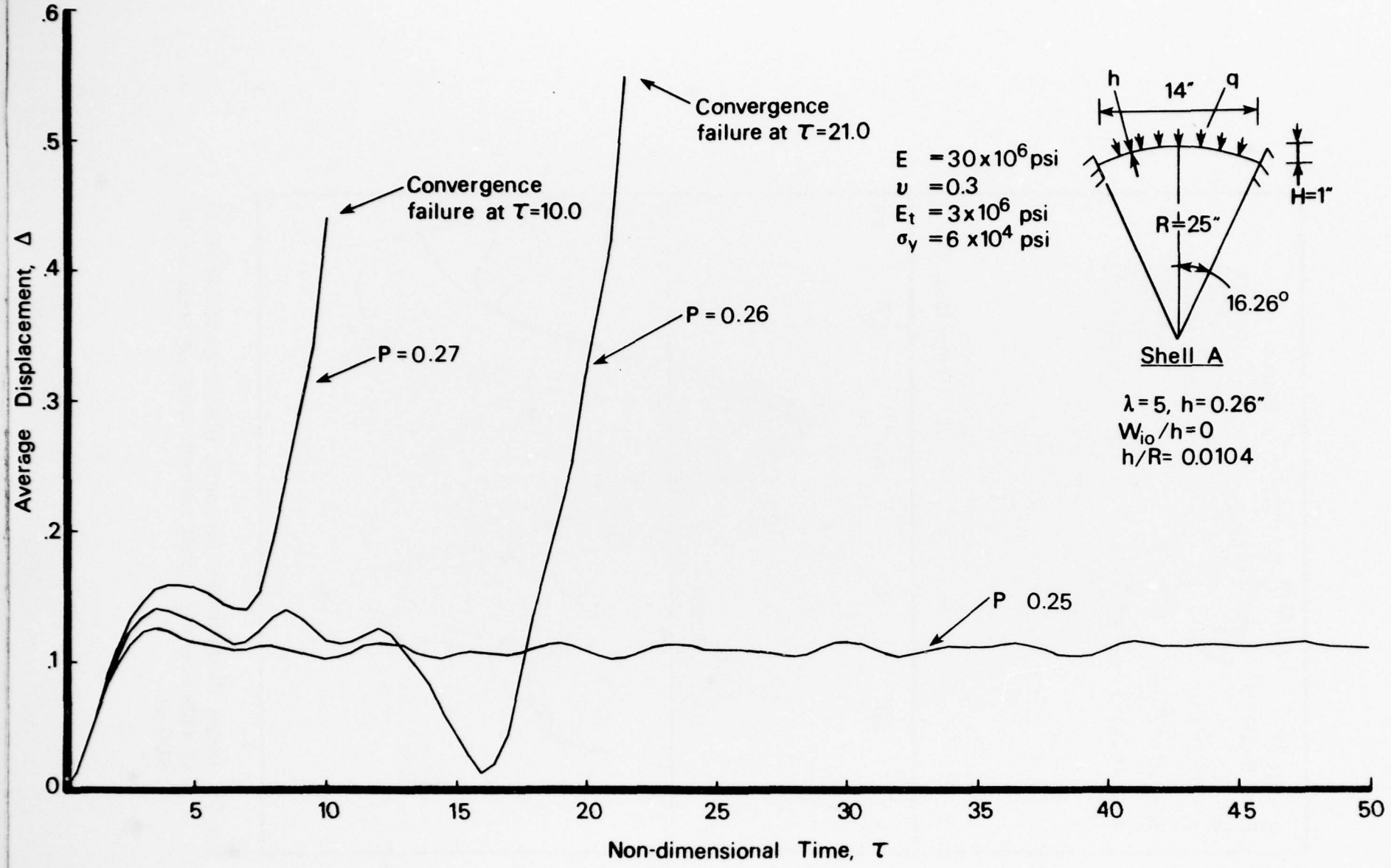

Fig. 7. Dynamic response for a clamped, elastic-plastic spherical cap ($\lambda = 5$) under uniform step pressure. (Shell A)

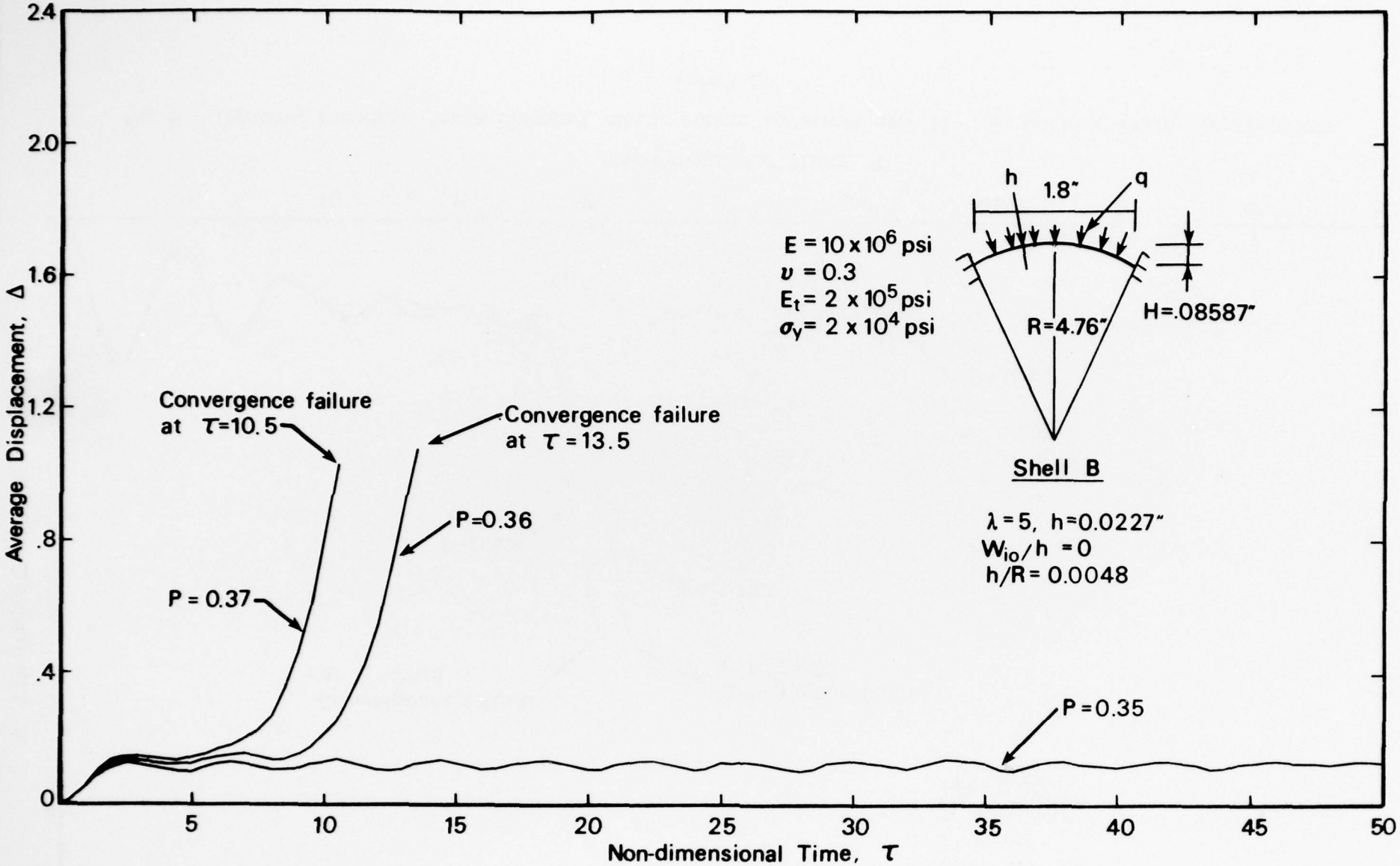

Fig. 8. Dynamic response for a clamped, elastic-plastic spherical cap (λ=5) under uniform step pressure. (Shell B)

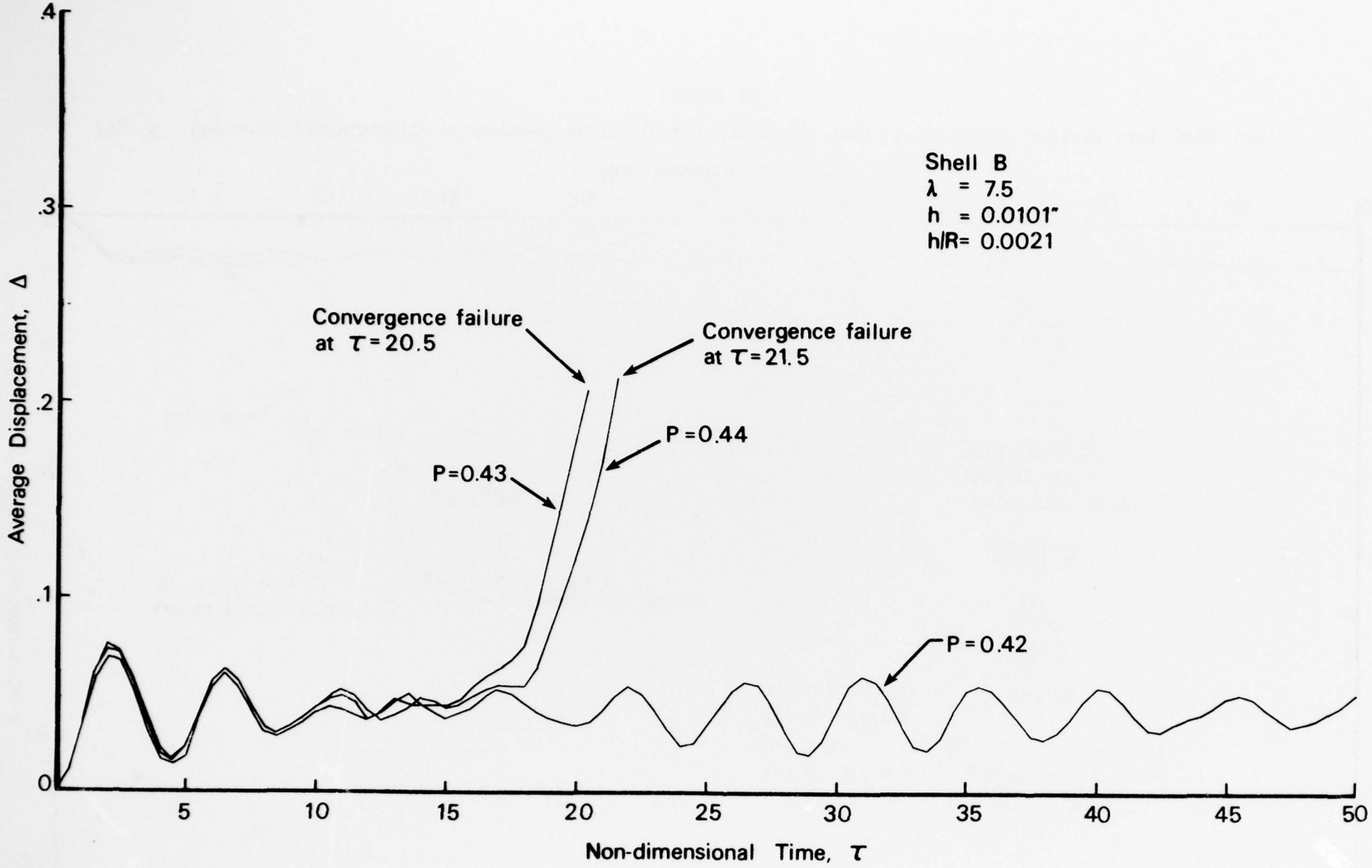

Fig. 9. Dynamic response for a clamped, elastic-plastic spherical cap ($\lambda = 7.5$) under uniform step pressure. (Shell B)

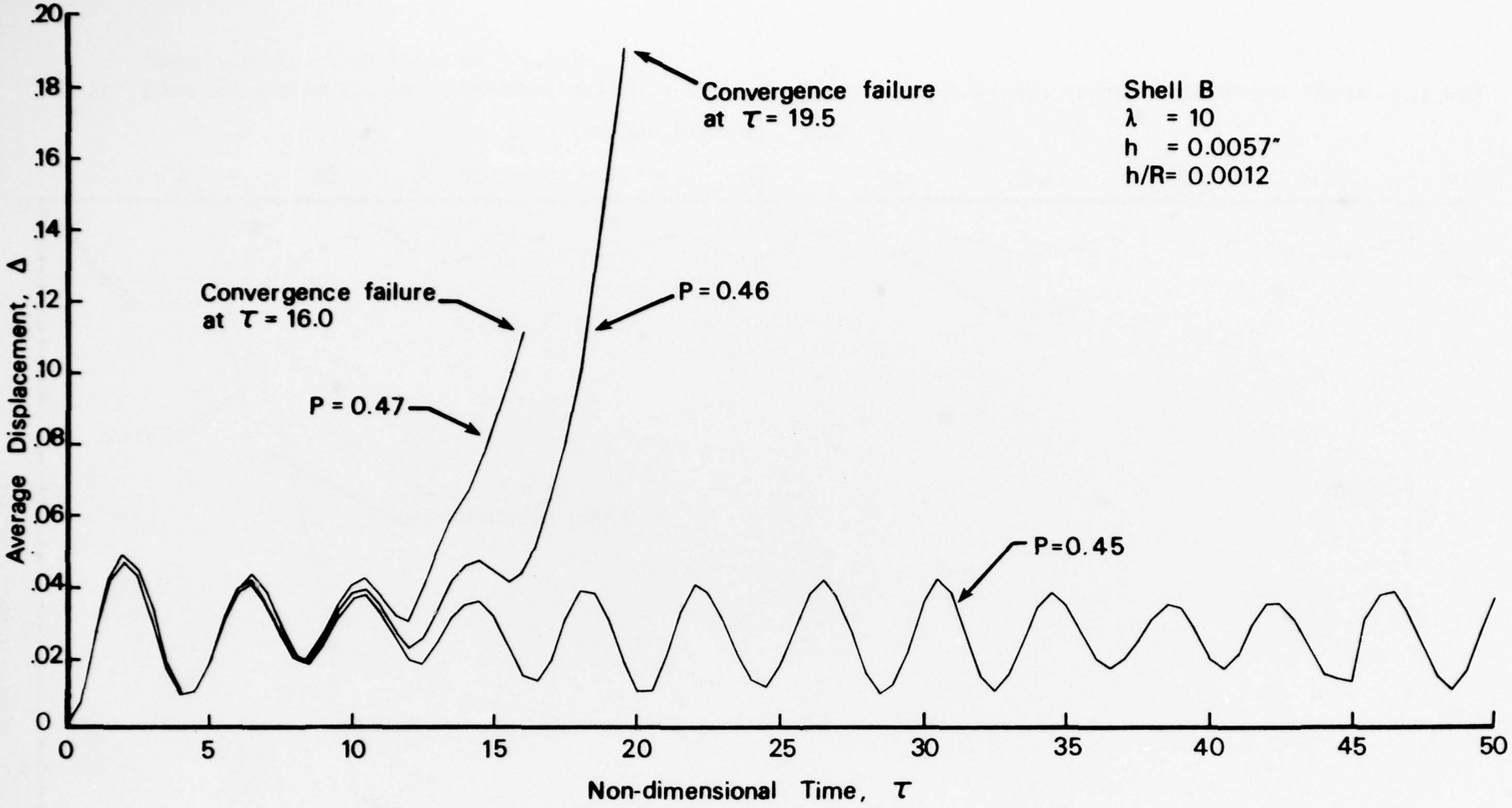

Fig. 10. Dynamic response for a clamped, elastic-plastic spherical cap ($\lambda = 10$) under uniform pressure.

(Shell B)

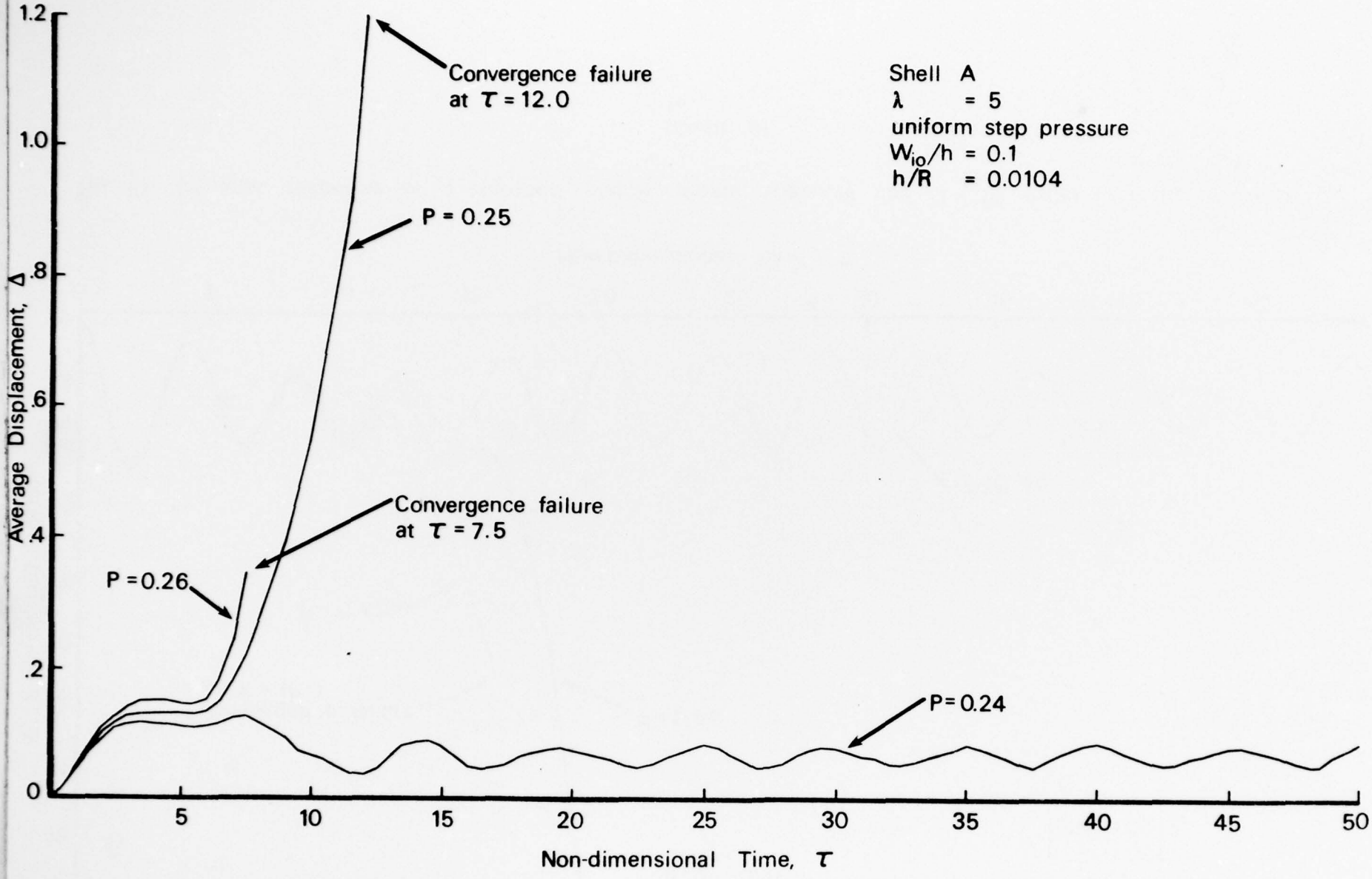

Fig. 11. Dynamic response for a clamped, elastic-plastic spherical cap ($\lambda = 5$) with initial imperfection $W_i/h = 0.1$ and under uniform step pressure (Shell A).

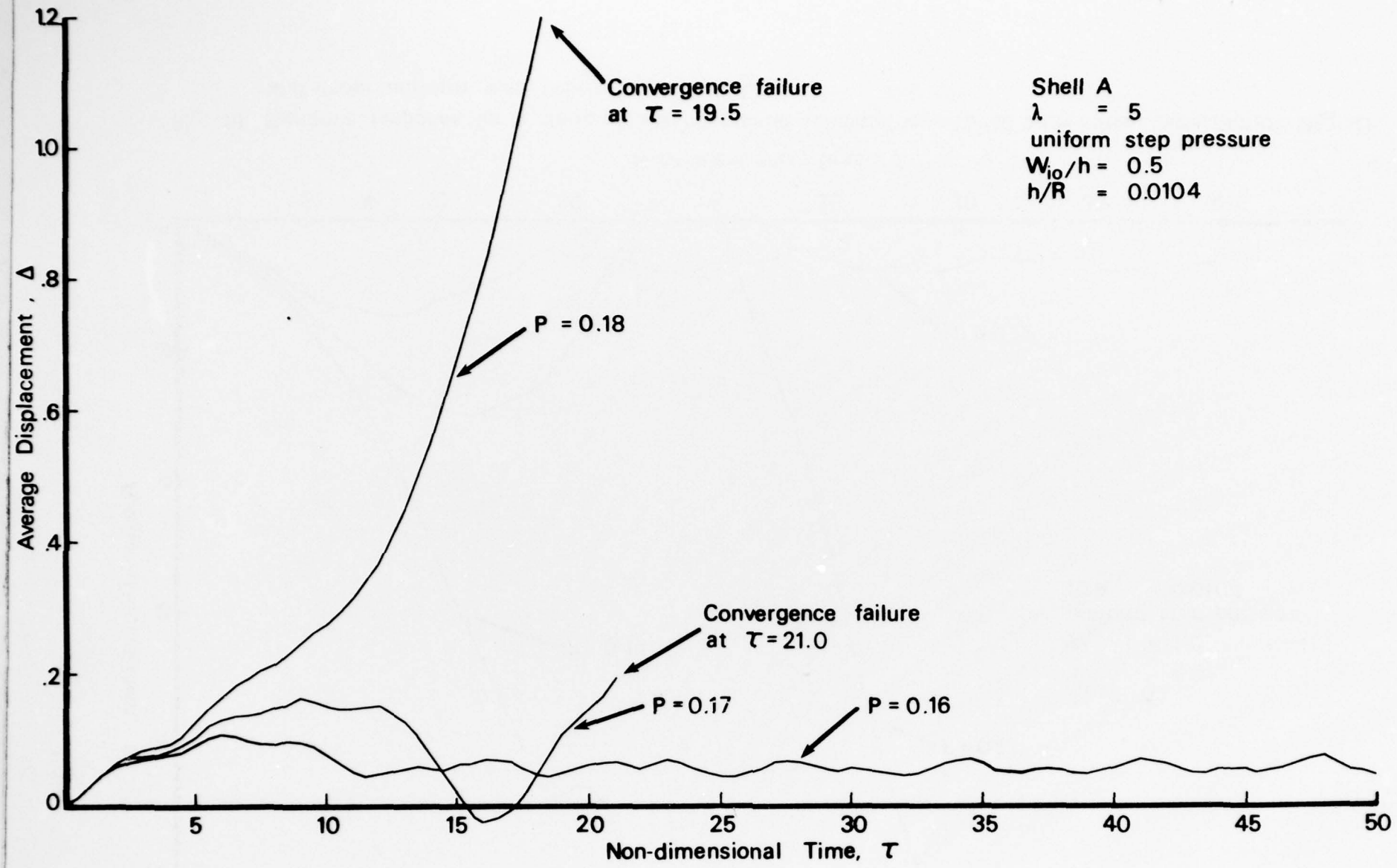

Fig. 12. Dynamic response for a clamped, elastic-plastic spherical cap (λ=5) with initial imperfection W_i/h =.5 and under uniform step pressure. (Shell A).

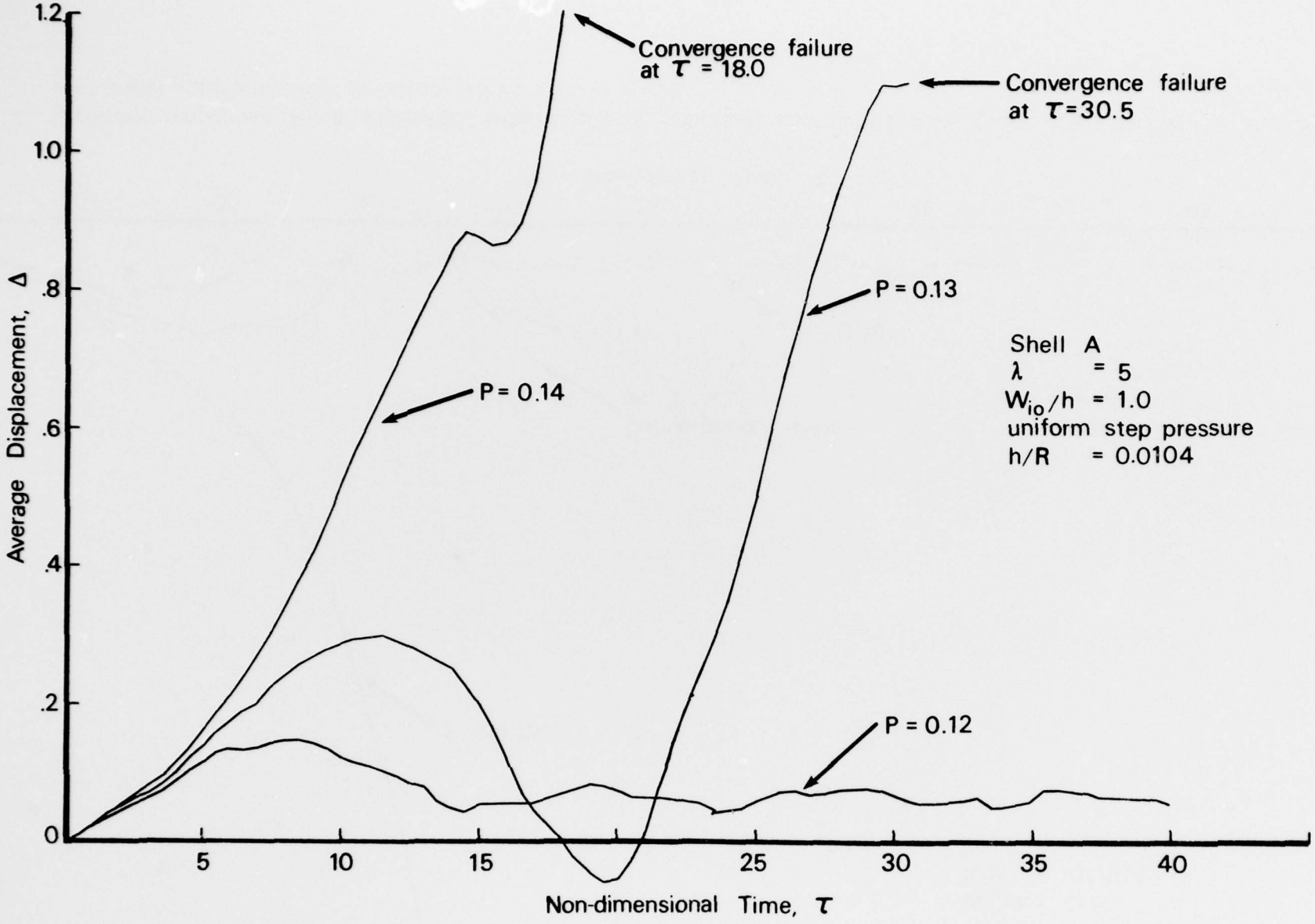

Fig. 13. Dynamic response for a clamped, elastic-plastic spherical cap ($\lambda=5$) with initial imperfection $W_{io}=1.0$ and under uniform step pressure. (Shell A).

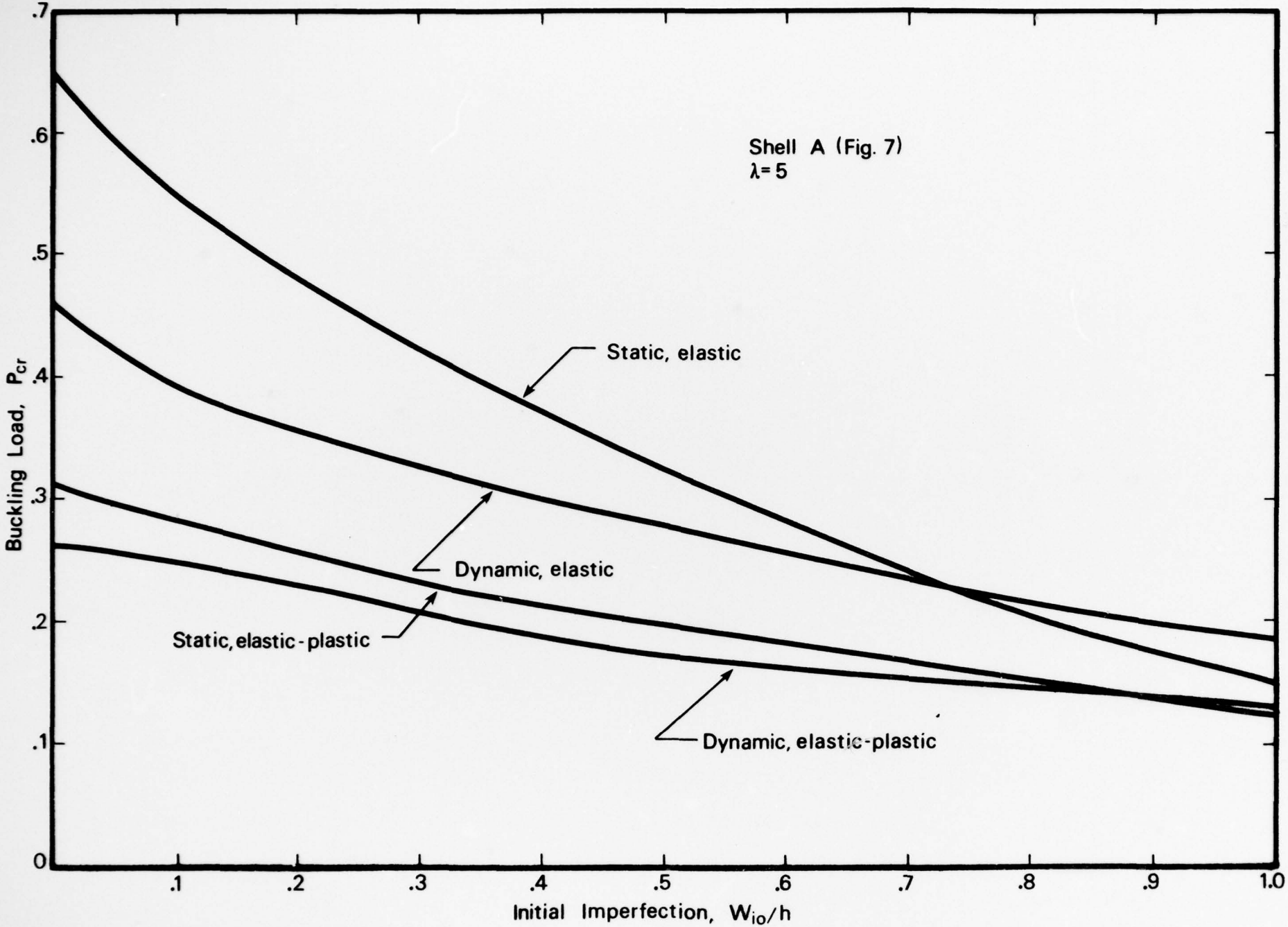

Fig. 14. Buckling load vs. initial imperfection for an axisymmetric spherical cap (Shell A, λ=5, Fig. 7).

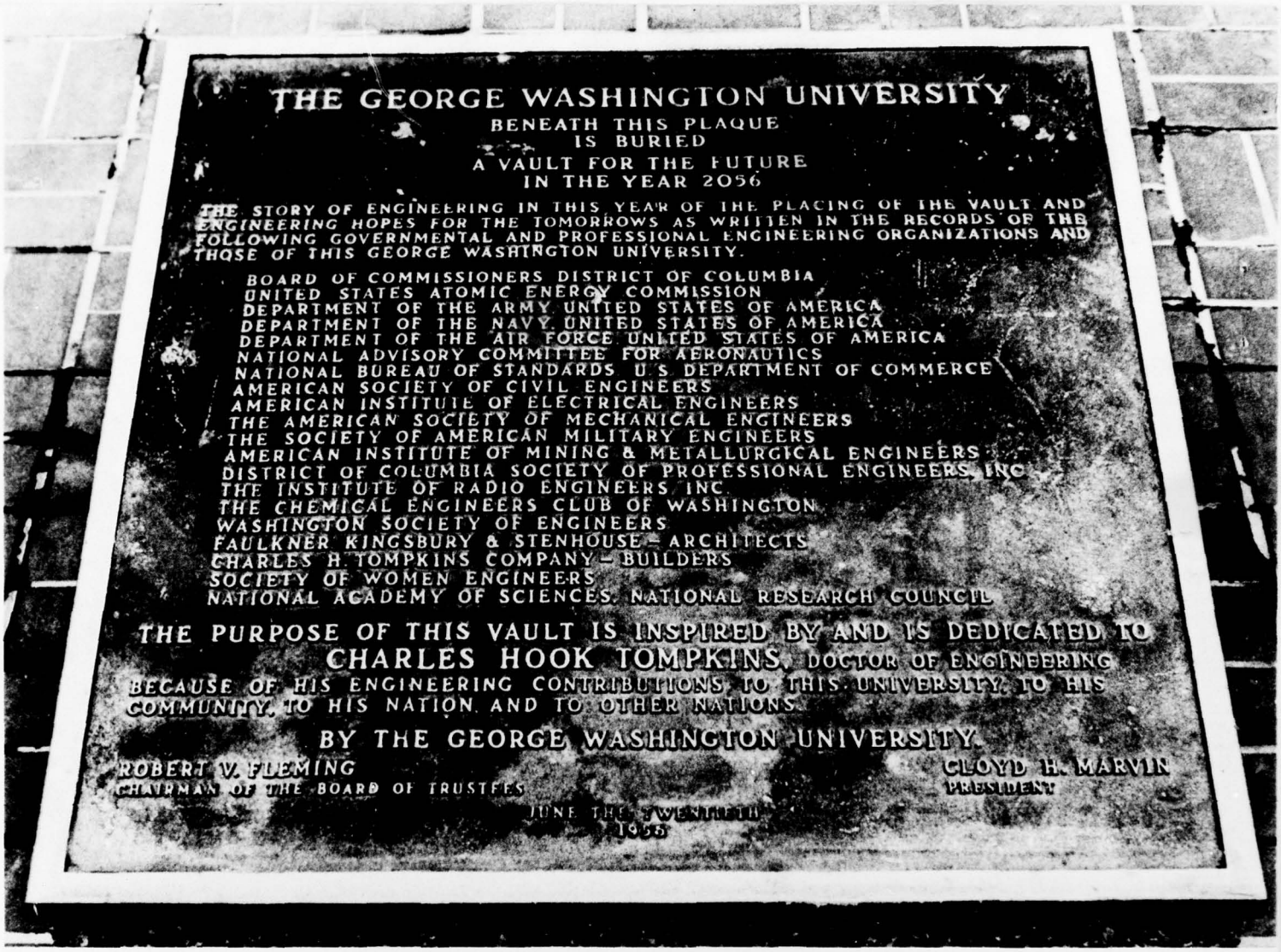

To cope with the expanding technology, our society must be assured of a continuing supply of rigorously trained and educated engineers. The School of Engineering and Applied Science is completely committed to this objective.